Fırat Üniversitesi Deneysel ve Hesaplamalı Mühendislik Dergisi

FUJECE

İntrakraniyal Kanama Tespiti İçin Segmentasyon Algoritmalarının Karşılaştırmalı Bir Çalışması

Murat CANAYAZ [1*], Aysel MİLANLIOĞLU[2], Sanem ŞEHRİBANOĞLU [3], Abdulsabır YALIN [4], Adem YOKUŞ [5]

[1]Bilgisayar Mühendisliği Bölümü, Mühendislik Fakültesi, Van Yüzüncü Yıl Üniversitesi, Türkiye.
[2,4]Nöroloji Bölümü, Tıp Fakültesi, Van Yüzüncü Yıl Üniversitesi, Türkiye.
[3]Ekonometri Bölümü, İktisadi ve İdari Bilimler Fakültesi, Van Yüzüncü Yıl Üniversitesi, Türkiye.
[5]Radyoloji Bölümü, Tıp Fakültesi, Van Yüzüncü Yıl Üniversitesi, Türkiye.
[1]mcanayaz@yyu.edu.tr, [2]ayselmilanlioglu@yyu.edu.tr, [3]sanem@yyu.edu.tr, [4]pamukkalet_@hotmail.com, [5]ademyokus@yyu.edu.tr

Geliş Tarihi: 22.01.2024
Kabul Tarihi: 14.03.2024
Düzeltme Tarihi: 10.03.2024
doi: https://doi.org/10.62520/fujece.1423648
Araştırma Makalesi

Alıntı: M. Canayaz, A. Milanlıoğlu, S. Şehribanoğlu, A. Yalın ve A. Yokuş, "İntrakraniyal kanama tespiti için segmentasyon algoritmalarının karşılaştırmalı bir çalışması", Fırat Üni. Deny. ve Hes. Müh. Derg., vol. 3, no 2, pp. 75-94, Haziran 2024.

Öz

Tıp alanında segmentasyon özel bir öneme sahiptir. Segmentasyonun amaçlarından biri, herhangi bir organdaki hastalık tespiti sonrasında hastalıktan etkilenen bölgeyi görselleştirmektir. Son yıllarda, bu amaçla derin öğrenme modelleri ile etkili çalışmalar gerçekleştirilmiştir. Bu çalışmada, beyin parankimindeki kanama tespiti için 3 segmentasyon algoritması karşılaştırılmıştır. Bu algoritmalar, en bilinen U-net, LinkNet ve FPN algoritmalarıdır. Bu algoritmaların arka planında, derin öğrenme modellerinden oluşan 5 farklı ana yapı kullanılmıştır. Bu ana yapılar, Resnet34, ResNet50, ResNet169, EfficientNetB0 ve EfficientNet B1'dir. Çalışma için orijinal bir veri kümesi oluşturulmuştur. Çalışmadaki veri kümesi uzmanlar tarafından doğrulanmıştır. Çalışmada, tıp alanındaki en yaygın metrikler olan Dice katsayısı ve Jaccard indeksi, değerlendirme metrikleri olarak seçilmiştir. Algoritmaların performans sonuçları göz önüne alındığında, eğitim verisi için FPN mimarisi 0.9495 Dice katsayısı değeri ile en iyi sonuçları verirken, test verisi için LinkNet 0.9244 Dice katsayısı ile en iyi sonuçları vermiştir. Ayrıca, kullanılan ana yapılar arasında EfficientNetB1 en iyi sonuçları sağlamıştır. Elde edilen sonuçlar incelendiğinde, mevcut çalışmalara göre daha iyi bir segmentasyon performansı elde edilmiştir.

Anahtar kelimeler: Bölütleme, İntrakraniyal kanama, Derin öğrenme

*Yazışılan yazar

İntihal Kontrol: Evet – Turnitin
Şikayet: fujece@firat.edu.tr

Firat Univ Jour. of Exp. and Comp. Eng., 3(2), 75-94, 2024

Firat University Journal of Experimental and Computational Engineering

A Comparative Study of Segmentation Algorithms for Intracerebral Hemorrhage Detection

Murat CANAYAZ [1*], Aysel MİLANLIOĞLU[2], Sanem ŞEHRİBANOĞLU [3], Abdulsabır YALIN [4], Adem YOKUŞ [5]

[1]Department of Computer Engineering, Faculty of Engineering, Van Yuzuncu Yil University, Türkiye.
[2,4]Department of Neurology, Faculty of Medicine, Van Yuzuncu Yil University, Türkiye.
[3]Department of Econometrics, Faculty of Economics and Administrative Sciences, Van Yuzuncu Yil University, Türkiye.
[5]Department of Radiology, Faculty of Medicine, Van Yuzuncu Yil University, Türkiye.
[1]mcanayaz@yyu.edu.tr, [2]ayselmilanlioglu@yyu.edu.tr, [3]sanem@yyu.edu.tr, [4]pamukkalet_@hotmail.com, [5]ademyokus@yyu.edu.tr

Received: 22.01.2024
Accepted: 14.03.2024
Revision: 10.03.2024
doi: https://doi.org/10.62520/fujece.1423648
Research Article

Citation: M. Canayaz, A. Milanlıoğlu, S. Şehribanoğlu, A. Yalın and A. Yokuş, "A comparative study of segmentation algorithms for ıntracerebral hemorrhage detection", Firat Univ. Jour.of Exper. and Comp. Eng., vol. 3, no 2, pp. 75-94, June 2024.

Abstract

Segmentation in the medical field has special importance. One of the purposes of segmentation is to visualize the area affected by the disease after disease detection in any organ. In recent years, efficient studies have been carried out for this purpose with deep learning models. In this study, three segmentation algorithms were compared for the detection of hemorrhage in brain parenchyma. These algorithms are the most familiar: U-net, LinkNet, and FPN algorithms. For the background of these algorithms, five backbones consisting of deep learning models were used. These backbones are Resnet34, ResNet50, ResNet169, EfficientNetB0, and EfficientNet B1. An original dataset was created for the study. The dataset in the study was verified by experts. In the study, the Dice coefficient and Jaccard index, which are the most common metrics in the medical field, were chosen as evaluation metrics. Considering the performance results of the algorithms, the FPN architecture with a 0.9495 Dice coefficient value for the training data and LinkNet with a 0.9244 Dice coefficient for the test data gave the best results. In addition, EfficientNetB1 provided the best results among the backbones used. When the results obtained were examined, better segmentation performance was obtained than in existing studies.

Keywords: Segmentation, Intracerebral hemorrhage, Deep learning

*Corresponding author

Plagiarism Checks: Yes – Turnitin
Complaints: fujece@firat.edu.tr

1. Introduction

Radiological data are primarily chosen by specialists for the detection of diseases. In these detection processes, faster results have been obtained with artificial intelligence and deep learning applications in recent years. With tools designed to assist experts, studies in the medical field continue to develop rapidly. These tools perform many functions, such as examining a given image and locating, segmenting, and recognizing the disease. These tools are used in the detection of many diseases, such as brain tumors [1], lung cancer [2], melanoma skin cancer [3], and diabetic retinopathy [4]. Non-traumatic spontaneous intracerebral hemorrhage (SIH) is an emerging disease of vascular origin in the brain that can cause high mortality and very serious functional disability, with an annual incidence of 25/1,000,000, accounting for 10-15% of all stroke patients [5, 6]. Systemic arterial hypertension, amyloid angiopathy, vascular malformation, and anticoagulant drug use are the most common risk factors [7]. Chronic arterial hypertension in patients causes lipohyalinosis and degenerative changes in penetrating arterioles over time. Charcot-Bouchard aneurysms occur in the posterior fossa, pons, basal ganglia, and thalamus localizations [8], which are deep brain structures, whereas in amyloid angiopathy, more amyloid depositions accumulate in the vessel wall with hemorrhages occurring in many lobar areas in the brain [9]. Pathophysiologically, it was determined that intracerebral hemorrhage causes compression in the surrounding neuronal tissue by creating a sudden and rapid mass effect in brain tissue, and neuronal injury is caused by damage to the signal pathways between neurons [10]. Non-contrast computed tomography (CT) is the gold standard neuro-imaging modality for the diagnosis of SIH due to its easy accessibility and rapid performance [11]. Although there is no definite and specific treatment, aggressive and early medical support, blood pressure regulation, intracranial pressure monitoring and control, management of secondary brain injury, prevention of complications, and, in selected cases, surgical intervention have positive effects on prognosis [12].

Intracerebral hemorrhage, which is a common disease, is an important disease that causes death if it is not detected. Therefore, rapid detection of the disease will increase the chances of early intervention. In our study, the aim was to present a rapid approach for the detection of this disease. For this purpose, different parameters and models were trialed to determine which of several segmentation algorithms would provide better results. Although the U-net model was used for intraparenchymal hemorrhage segmentation in studies, segmentation algorithms such as LinkNet and FPN were not used, providing significant motivation to our study in terms of showing the performance of these algorithms. While ready-made datasets were used in other studies, data labeled by experts in the field was used in our study. For the reliability of success in measuring accurate performance, images related to this disease provided by RSNA [13] were included in our study, as well as our own dataset. The originality of our dataset, which is among the innovative aspects of our study, and the ability to detect disease with high accuracy rates by using multiple segmentation algorithms trained with different models are important criteria that distinguish our study from other studies. The contributions of our study to the field can be listed as follows:

- A new publicly available dataset showing expert-labeled intracranial intracerebral hemorrhage.
- Investigation of the performance of multiple segmentation algorithms and different backbones applied for the first time for this disease.

The organization of our study is as follows: in the second part, studies related to the disease are given. The methodology is given in the third section, and the results are given in the fourth section. The last sections contain the discussion and conclusion.

2. Related Works

In this section, firstly, segmentation studies on intracerebral hemorrhage detection and then classification studies are examined in detail. In the last part, studies in the medical field with the models we used in our study are given.

Accurate segmentation and quantification of intraparenchymal hematoma is very important to be able to diagnose patients more quickly and at a higher rate, to predict the outcomes for patients more accurately with the correct estimation of bleeding volume, and to decide on treatment options [14]. In recent years, studies

estimated bleeding volume very rapidly using segmentation algorithms, treatment strategies were developed, and more accurate and stable performances were achieved by using different methods [15–17]. Falk et al. presented an ImageJ plugin to analyze cell detection and shape measurements in U-net [18]. Hu et al. proposed an encoder-decoder convolutional neural network (ED-Net) for the detection of intracerebral hemorrhage (ICH). The model they propose makes extensive use of both low-level and high-level semantic knowledge. Although they achieved good results in their studies, they stated that their models still do not take into account spatial information, and this is a limitation of their work. It was stated in their studies that a dice coefficient of over 80% and a Jaccard index of over 75% were obtained [17]. Arab et al. attempted to develop a fast and fully automated deep learning method that applied deep supervised convolutional neural networks (CNN-DS) for hematoma segmentation and volume measurement in CT scans. They compared CNN-DS with three different methods and obtained the best result of 0.84 for CNN-DS. It was mentioned in their studies that more labeled data is needed for the detection of hematoma and that there may be human-induced errors while labeling. In our study, the tagged dataset was validated separately by three of our experts to minimize human-induced errors [19]. Jadon et al. used different image segmentation models (U-Net 2D, Inception-based UNet++ 2D model) to segment different phenotypes of hemorrhagic lesions in their study. In their study, they obtained a Dice coefficient of 0.94 for intraparenchymal hemorrhage (IPH) by using the Focal Tversky Loss Function in the UNet++ 2D model. This is a study showing the effect of the loss functions we used in our study on segmentation [20]. Cao et al. used the fuzzy C-means clustering method to separate the pixels on CT images and used the U-Net neural network they developed for auxiliary diagnosis of intracerebral hemorrhage. In the study, pixels in CT images are divided into four categories: white matter, gray matter, cerebrospinal fluid, and hemorrhage. The fact that this requires pre-processing before segmentation can be seen among the limits of the study. In the study, a 0.860 Dice coefficient value and a 0.712 Jaccard value were obtained [21]. Wang et al. proposed a modified U-Net and curriculum learning strategy to distinguish ICH subgroups on CT images. They emphasized that more training should be done with more data in their studies, where they obtained low values such as 0.67 Dice Coefficient and 0.50 Jaccard value [22]. Maya et al. classified the hemorrhage region into 3 types (epidural, subdural, and intraparenchymal hemorrhage) in their study using U-Net and CapsNet on CT images with stroke symptoms. In the study, first of all, some image processing methods were applied to the images. Then segmentation was done with U-net. In this segmentation, 75% Dice coefficent was obtained. Segmented images were classified with CapsNet. 92.1% validation accuracy was achieved with CapsNet [23]. Hssayeni et al. used an ICH segmentation method based on 5-fold cross-validation in their study, where they developed a deep fully connected network (FCN) named U-Net to segment ICH regions on CT scans in a fully automatic manner. It has been reported that a Dice coefficient of 0.31 was obtained in this segmentation process. They emphasized that this low dice coefficient value may be due to incorrect segmentation near the bone in grayscale images where the density is similar. They also stated that the model they developed in the study was not sufficient to detect small hemorrhages [24]. Abramova et al. used a 3D U-Net architecture with compression and excitation blocks to automatically segment hemorrhagic stroke lesions on CT scans, as well as restrictive patch sampling to alleviate the problem of class imbalance and resolve the issue of intraventricular hemorrhage not considered to be a stroke lesion. The average Dice coefficient value of 0.86 was reached in the study. It has been stated that the performance of U-net increases when used with squeeze-and-excitation blocks [25]. Liu et al. used the U-Net neural network model and contour recognition to extract the brain parenchymal region through intelligent tissue analysis of cerebral hemorrhage after segmentation to detect hypertensive intracerebral hemorrhages. It contributes to this field as a study that provides texture analysis after segmentation [26]. Manasa et al. used the U-Net algorithm for semantic segmentation in a study using 146 images for the detection of ICH [27].

He (2020) used SE-ResNeXt50 and EfficientNet-B3 to learn the classification for five subtypes of intracranial hemorrhage. The RNSA dataset, which is also included in our study, was used here. A classification has been made for all diseases in this dataset. As a result of classification, a 0.0548 loss score value was obtained in test sets [28]. Castro et al. used VGG-16 and CNN-4 for detection of intracranial hemorrhage (HIC). In their study, they made a classification that only states whether there is hemorrhage or not. For this binary classification, the accuracy rate they obtained with VGG-16 was 0.968, and the accuracy rate they obtained with CNN-4 was 0.981. As a result, they reported that CNN could be a useful tool for CT images in disease detection [29]. Burduja et al., in their intracranial hemorrhage detection study based on the RSNA 2019 dataset with CTs, used a lightweight deep neural network architecture consisting of a

convolutional neural network (CNN) and a long short-term memory (LSTM) network. In their studies, they tried to classify the feature vectors they obtained from the images. It has been stated that an accuracy of over 96% has been achieved. In the limitations of the study, they demonstrated that their system was able to predict the correct label for a particular bleeding subtype without considering all sites for the relevant subtype. They concluded that although this behavior produces very good accuracy rates, it is not optimal for visualizing all bleeding sites. In our application, an accurate visualization of the bleeding site is provided [30].

Araújo et al. used a melanoma segmentation method based on U-Net and LinkNet deep learning networks combined with transfer learning and fine-tuning techniques. Additionally, they evaluated the model's ability to learn to segment the dataset by merging the disease or just the datasets. The experiments were performed on three datasets (PH2, ISIC 2018, and DermIS), and they stated that they obtained more promising results with U-net, whose Dice values averaged 0.923 in the PH2 dataset, 0.893 in ISIC 2018, and 0.879 for DermIS, respectively. Although there is no ICH segmentation in the study, it is one of the studies in which the performance comparisons of U-net and LinkNet are included [3]. Ghosh et al. detected brain tumors by comparing two different U-Net architectures (U-Net: baseline and U-Net: ResNeXt50 backbone) and a feature pyramid network (FPN) based on segmentation. The U-Net architecture with the ResNeXt50 backbone achieved dice coefficients of 0.932, with values for basic U-Net and FPN of 0.846 and 0.899, respectively. In this study, U-net and FPN were used together. It is also seen that a better dice coefficient value can be obtained by using the ResNeXt50 backbone for U-net [31]. Sobhaninia et al. measured some biometric parameters, such as fetal head circumference (HC), to check the health and growth of the fetus. For this study, they used mini-LinkNet by modifying LinkNet as a multiscale light convolutional neural network. In this study, the effective structure of LinkNet is emphasized [32]. In their study using a cross-scale feature pyramid for OCT images, Fan et al. achieved an average sensitivity (mAP) of 85.02 for FPN for OCT lesion detection [33]. Dai et al. used cone-beam CT (CBCT)-based adaptive radiotherapy in their study, in which they automatically identified at-risk head and neck organs using dual pyramid networks. When the results of the patient images were examined, the best DSC was 0.96 for the oral cavity and 0.66 for the lowest optical chiasm [34]. Lo et al. proposed a deep learning (DL) framework for 2D fetal MRI segmentation using a cross-attention squeeze excitation network (CASE-Net) for research and clinical applications. The purpose of CASE-Net was to emphasize the localization of contextual information related to biomedical segmentation by combining attentional mechanisms with squeezing and excitation (SE) blocks. This was a retrospective study with 34 patients. In their experiments, they showed that the proposed CASE-Net outperformed other competitive segmentation architectures, achieving the highest segmentation Dice score of 87.36% [35]. Singh et al. used the ImageCLEF Med Tuberculosis 2019 dataset in their study about detecting tuberculosis lesions in the lungs using image segmentation. The dataset consisted of 3D CT images divided into 2D slices, and segmentation was applied to each slice using U-Net, FPN, and LinkNet architectures. In this study, three segmentation algorithms were compared, as in our study [36].

3. Methodology

3.1. Dataset

In our study, the data of 100 patients (44 males and 56 females) diagnosed with SIH who were hospitalized in the Neurology Department of Van Yüzüncü Yıl University were analyzed retrospectively. All permissions for the study were obtained from the hospital ethics committee. The mean age of the patients was 65.1 years (23–95 years). Patients with epidural, subdural, subarachnoid, ventricular hemorrhages, aneurysms, or hematomas secondary to vascular malformations were excluded from the study. In CT imaging, hematoma is easier to recognize because it appears brighter (hyperintense) than the surrounding brain tissue and cerebrospinal fluid. The ABC/2 formula, which is frequently used in clinical studies and daily practice, was used to calculate the hematoma volume. Using the ABC/2 formula, total hematoma volumes were calculated with perpendicular diameter measurements from CT images in both coronal and axial planes. These calculations were made independently by two neurologists in order to reduce observer variability and measure the hematoma volume as if it were larger than it is, especially in irregular hematomas. The hematoma volume average was 45.3 cm3 (0.49–273 cm3). For the segmentation process, both the images in the dataset and the contours of the hematoma on the CT images of the patients were manually marked with a red color by the neurologists using the cursor.

In order to contribute to the dataset in our study, 264 intracerebral hemorrhage images were identified from the RNSA [13] dataset. This dataset was created by four working groups consisting of Stanford University, Thomas Jefferson University, Unity Health Toronto, Universidade Federal de São Paulo (UNIFESP), and the American Society of Neuroradiology (ASNR) [13]. In the dataset, there are images of other intracranial hemorrhages. Among these, images that were confirmed as intracerebral hemorrhages were selected for use in our study. The selected images were again marked by our experts. Ground truth masks were removed from the marked images. Examples of images marked and unmasked by experts are given in Figure 1.

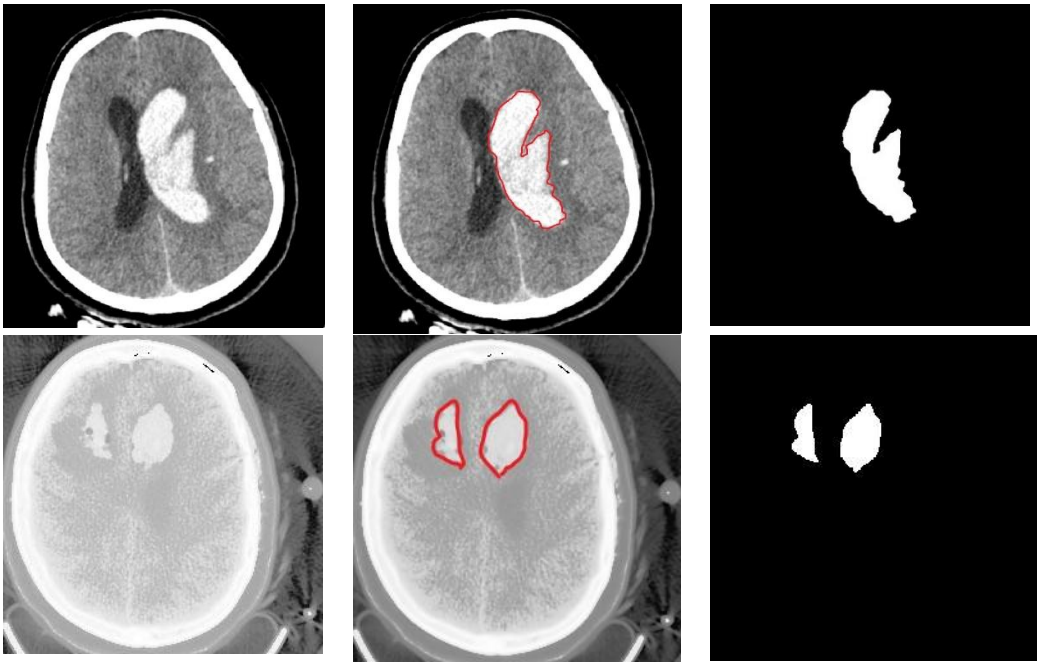

Figure 1. Samples from the Dataset

In Figure 1, the first row shows an example from the first dataset, and row 2 shows an example from the RNSA dataset. As can be seen, the second dataset has lower values in terms of both resolution and quality than the first dataset.

3.2. Segmentation Algorithms

3.2.1. U-Net

The architecture known as the Fully Convolutional Network (FCN) stands out as a remarkably successful and frequently employed foundational structure recommended for semantic segmentation [37]. U-Net, another architectural framework derived from FCN, was specifically devised for the semantic segmentation of medical images [38]. The network's structure comprises two distinct segments, namely the contraction and expansion paths [26, 38]. Operations conducted on the left side, the contraction path, aim to grasp contextual details of the image, effectively extracting features from it. These operations closely adhere to the established logic of classical CNN architecture.

Conversely, operations on the right side, the expansion path, precisely localize the segments within the image [38, 39]. The connection between the contraction and expansion paths employs a concatenation operator instead of summation, enhancing the direct application of spatial information to deeper layers and achieving a more precise segmentation outcome [40]. Unlike classical deep learning, which requires abundant examples and substantial computing resources, U-Net demonstrates adaptability with minimal training sets [39, 41]. Notably, this adaptability renders it particularly suitable for tasks involving the segmentation of medical images [39, 42].

U-Net's distinctive strategy, which sets it apart from other segmentation architectures, involves combining feature maps from the contraction phase with their symmetrical counterparts in the expansion phase. This innovative approach facilitates the dispersion of contextual information into high-resolution feature maps [3]. The structural depiction of U-Net is illustrated in Figure 2.

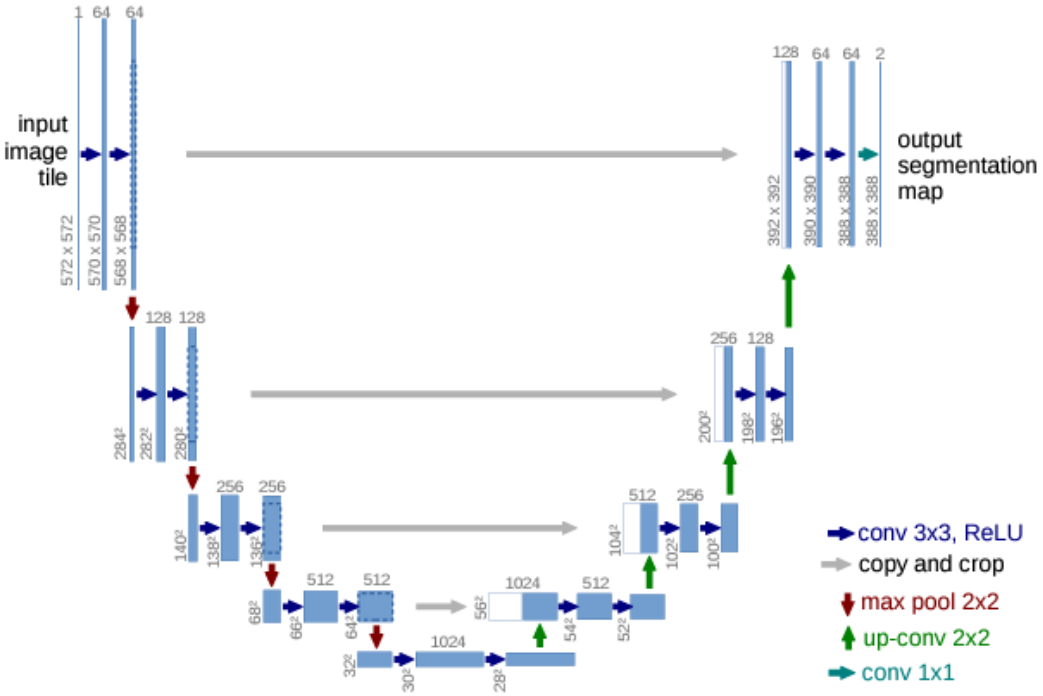

Figure 2. U-net Structure [38]

3.2.2. LinkNet

LinkNet features a streamlined deep neural network architecture that facilitates the acquisition of knowledge in semantic segmentation tasks without a notable surge in parameters. It bears resemblance to U-Net and other segmentation networks. Positioned on the left is an encoder, while on the right is a decoder [3]. The encoder operates by encoding data within the source space, and the decoder translates this data into spatial categorization to execute the segmentation [3, 43]. Unlike current neural network architectures, where encoders in segmentation processes perform multiple downsampling operations, LinkNet adopts a different approach. This deviation is crucial, as the conventional process tends to result in the loss of spatial information during cascading convolutions in the encoder segment [44]. Retrieving such lost information proves to be challenging [43].

In Link-Net, a distinctive feature is observed wherein the input of each encoder layer is concurrently assigned to the output of the corresponding decoder. The intent behind this mechanism is to reclaim spatial information that was lost, serving as a valuable resource for the decoder and the subsequent upsampling processes [43]. The utilization of fewer parameters is a noteworthy characteristic, attributed to the shared information learned by the encoder, facilitated by the decoder [36, 43]. Figure 3 illustrates the structural layout of LinkNet.

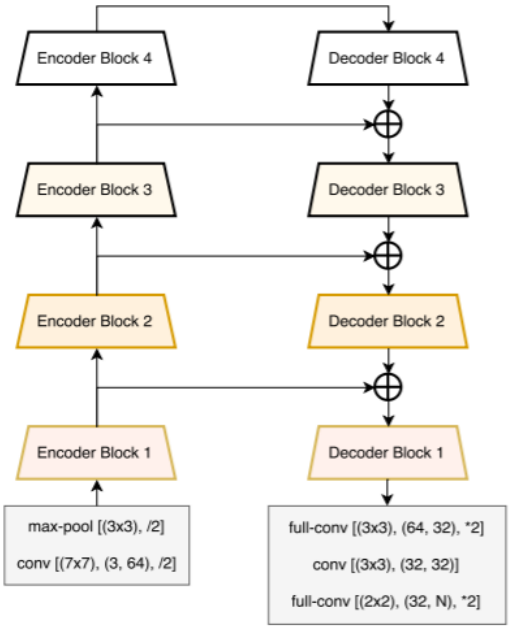

Figure 3. LinkNet Structure [43]

3.2.3. FPN

FPN utilizes the pyramidal hierarchy of deep convolutional networks to generate feature pyramids with minimal additional computational cost [45]. Image pyramids serve as a data structure specifically designed to facilitate convolution by employing downscaled versions of the original image at regular intervals. These downscaled copies effectively reduce both sample density and resolution [46]. The foundational concept of feature pyramids is established by image pyramids [47]. The pyramid framework is believed to offer a conceptual unification for representing and manipulating low-level visual information. It presents a versatile and convenient multi-resolution format that aligns with various scales present in visual scenes, mirroring the multiple processing scales within the human visual system [46]. FPN, functioning as a feature extractor grounded in the pyramid concept, excels in both accuracy and speed [47]. While ConvNets provide a high level of semantic understanding and resistance to variance, the inclusion of pyramids remains essential for achieving optimal accuracy. Specifying each level of an image pyramid yields a multi-scale feature representation where all levels, including those with high resolution, exhibit significant semantic strength. However, the drawback of employing an image pyramid lies in the increased extraction time [47].

FPN employs a comprehensive approach, combining features through bottom-up, top-down paths, and lateral connections to leverage the feature hierarchy, ultimately creating a robust feature pyramid [48]. The bottom-up path facilitates a top-down progression, rendering higher-resolution layers compared to the base layer. Each stage in this progression is identified as a pyramid level [46]. Among the reconstructed layers, the final layer output is selected as a feature map to construct the pyramid [47]. The top-down path is enriched by incorporating lateral links between feature maps [36]. This path creates spatially coarser yet semantically stronger feature maps with higher-resolution layers in a top-down manner. These features are further enhanced by integrating features from the bottom-up path through lateral links. Each lateral link connects feature maps with the same spatial dimensions from both the bottom-up and top-down paths [47]. The structural representation of FPN is visually depicted in Figure 4.

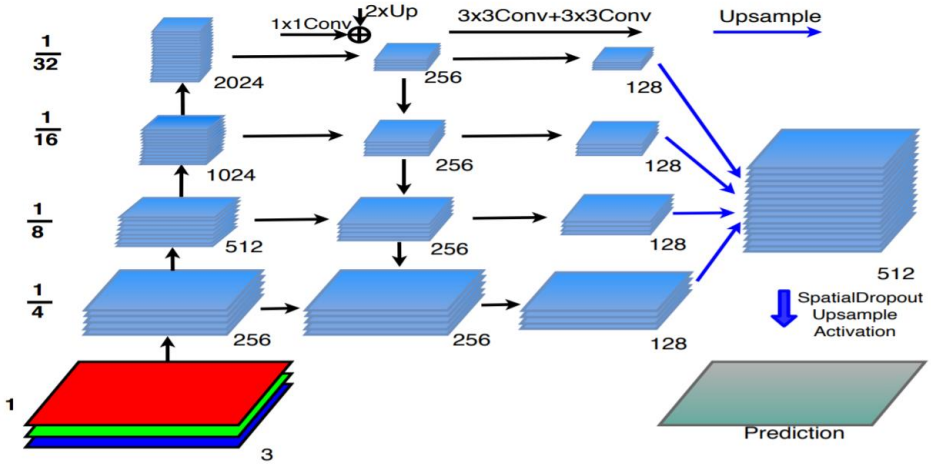

Figure 4. FPN Structure [45]

3.3. Backbones

3.3.1. ResNet

Residual Network (ResNet) [49] is a deep learning network architecture using residual layers that won first place in the ImageNet competition in 2015. In this model, it is thought that a faster model will be created by adding residual values between the linear and ReLU layers and the blocks that feed the next layers (residual blocks). For this reason, in network structures where the residual block structure is used, the data in one layer is given as input to the next layer and transmitted to the next layers in 2 or 3 layers. The single residual block structure is shown in Figure 5. The output of the residual block can be formulated as in Equation 1.

$$y = F(x) + x \tag{1}$$

where F is the residual function and x and y are the input and output of the residual function, respectively. The entire residual network consists of the first convolutional layer and a few basic blocks [50]. The structure of the ResNet 34 model is shown in Figure 6 [49].

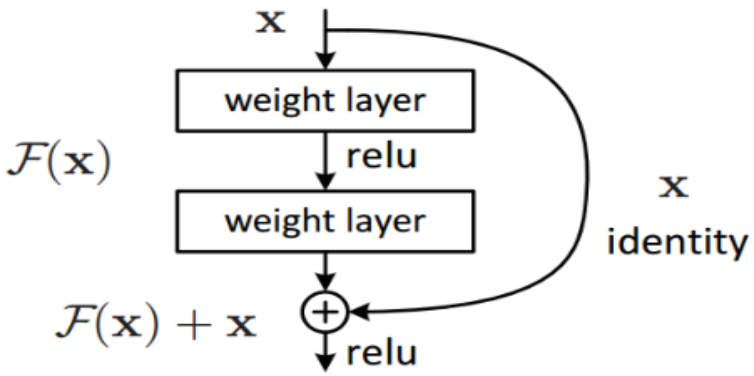

Figure. 5. Single residual block [49]

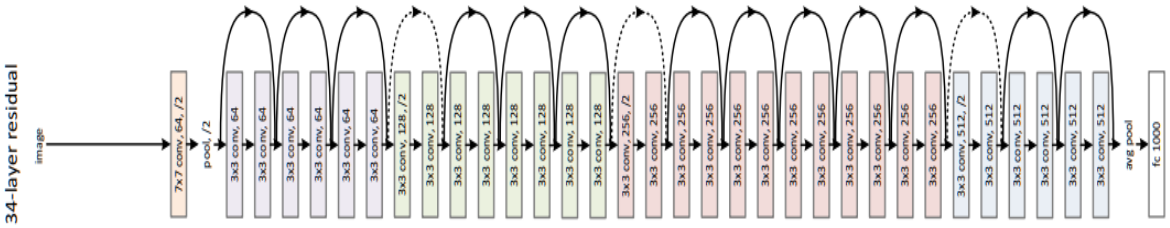

Figure. 6. ResNet34 Structure

3.3.2. EfficientNet

EfficientNet is a deep learning model developed by the Google research team [51] in 2019. There are many different versions of this model, from B0 to B7, which were developed based on the hypothesis of increasing the width and resolution of the model as well as the depth of the model. As the number of parameters calculated in each version increased, the computational cost also increased. While performing EfficientNet, the ResNet model was used for the first performance comparisons. In our application, these models were selected as the backbones for segmentation algorithms, and performance comparisons were made. The three concepts this model considers are depth, breadth, and resolution. Depth refers to how deep the meshes are. In other words, it is equivalent to the number of layers. The width is the number of channels in the convolution layer. Resolution is the resolution of the image transmitted to the network. Researchers proposed a new scaling method that equally scales all dimensions of the network's depth, width, and resolution. We can summarize these concepts in Figure 7 [51].

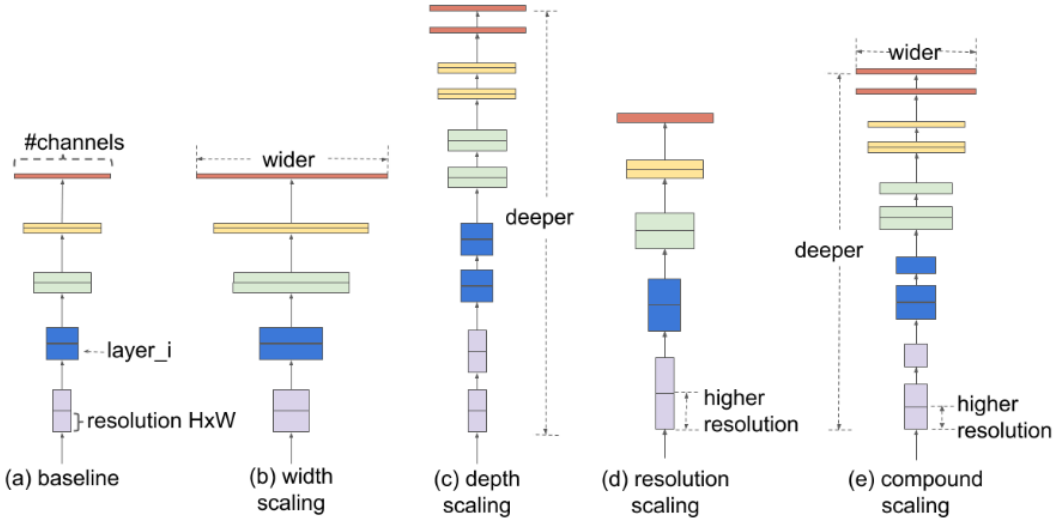

Figure 7. a) Basic network example, b)-d) traditional scalings that increase only one dimension of network width, depth or resolution, e) EfficientNet's composite scaling method

The EfficentNet B0 structure is shown in Figure 8. The main building block of this mesh is MBConv, to which compression and excitation optimization are added. These blocks create shortcuts between the beginning and end of a convolutional block. Input activation maps are expanded using 1x1 convolutions, increasing the depth of feature maps. The shortcut links used in this model connect narrow layers together, while wider layers are located between jump links. This structure helps reduce the model size as well as the total number of operations required. Other parameters used in this model are as follows: kernel_size is the kernel size for convolution, for example, 5 x 5; num_repeat specifies that the repeat count of a given block must be greater than zero; input_filters and output_filters are the number of filters; expand_ratio is the input filter expansion rate; id_skip determines whether to use link skipping; and se_ratio shows the spin rate for squeezing and excitation blocks.

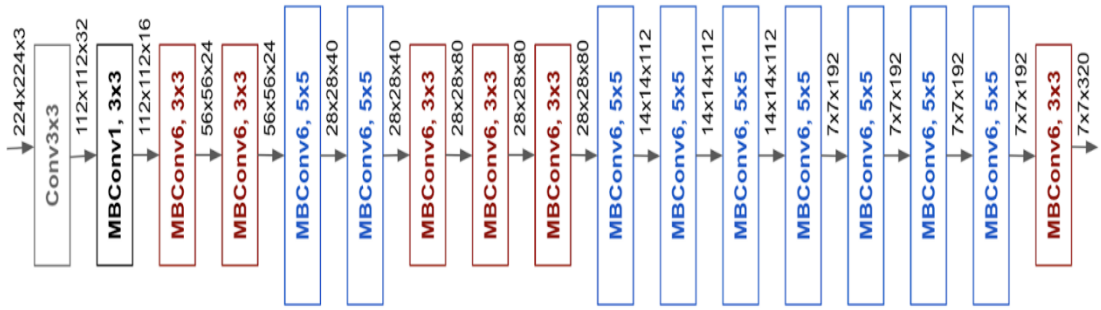

Figure 8. EfficientNet B0 Structure [51]

3.4. Application

The Python environment was used for the application. Before the application, 334 images in the dataset were reserved for model training, and 30 images were used for performance analysis after model training was completed. During the model training process, 20% of 334 images were used for validation. The dataset was run separately in each segmentation algorithm. Different backbones were tested in each run. At the end of the run, performance analysis was made for the models with test data. The parameter values used in the operation of the models are given in Table 1.

Table 1. Parameter Settings

Parameter	Value
Optimizer	Adam
Learning Rate	0.0005
Epoch	100
Batch Size	8
Input Size	(256,256,3)
Activation	Sigmoid
callbacks	ReduceLROnPlateau and ModelCheckPoint

4. Evaluation Metrics

The application was run on a workstation with an I7 processor and 16 GB of RAM. The workstation had a graphics card with a Geforce 1070 GPU. Evaluation metrics are covered in two different sections. The first of these is the segmentation metric that is needed to examine the segmentation results, while the second is the model metrics used to examine the accuracy of the models.

4.1. Segmentation Metrics

4.1.1. Jaccard Index

The Jaccard index is a metric that measures the similarity between the reference value and the predicted value in segmentation applications. For this metric value, similar features between the two values are divided into the union of the two sets; in other words, by taking the intersection of the two sets. The formula used for the Jaccard index is given in equation 2. This metric ranges from 0–1 (0–100%); 0 indicates no overlap, and 1 indicates perfectly overlapping segmentation.

$$J(Y,Y') = \frac{|Y \cap Y'|}{|Y| + |Y'| - |Y \cap Y'|} \tag{2}$$

Where Y is the ground truth and Y' is the prediction.

4.1.2. Dice Coefficient

This metric is very similar to the Jaccard index. There is a positive relationship between them. It is a well-known metric that measures the similarity between the reference value and the predicted value in segmentation. Like the Jaccard index, this metric has values between 0 and 1, where 0 indicates no overlap and 1 indicates perfectly overlapping segmentation. Equation 3 is used for the Dice coefficient.

$$J(Y, Y') = \frac{2|Y \cap Y'|}{|Y| + |Y'|} \tag{3}$$

Where Y is the ground truth and Y' is the prediction.

4.2. Model Metrics

4.2.1. Binary Cross Entropy Loss

This loss function is used in binary classification tasks. As is known, masks used consist of binary images as background 0 and foreground 1. Equation 4 is used for this function.

$$L_{BCE}(y, \hat{y}) = -(ylog(\hat{y}) + (1 - y)\log(1 - \hat{y})) \tag{4}$$

Here $\hat{y}$ denotes the value predicted by the model and y is the target value.

4.2.2. Dice Loss

Dice is a loss function often used to evaluate success in biomedical images. Equation 5 is used for this function.

$$\text{DiceLoss} = -\frac{2}{|C|}\sum_{i}^{C}\frac{\sum_k S_i^k L_i^k}{\sum_k S_i^k + \sum_k L_i^k} \tag{5}$$

Where C is the number of classes, k is every pixel in the image, S is the prediction and L is the ground truth label.

4.2.3. Focal Loss

Loss of focus (FL) [52] attempts to reduce the contribution of easy examples so that CNN can focus more on difficult examples. It does this by giving more weight to samples that are difficult or easily misclassified. Focal loss is included in the literature as a more developed version of cross-entropy. Therefore, Equation 6 was used to calculate the focal loss.

$$FL(p_t) = -(1 - p_t)^{\gamma}\log(p_t) \tag{6}$$

As can be seen from the formula, it adds the factor $(1 - p_t)^{\gamma}$ to cross-entropy. Relative loss is reduced for samples classified well when γ>0.

5. Results

It is possible to evaluate the results of our study as an ablation study. Two different threshold values were used for the Jaccard index and Dice coefficient values in the study. These are values of 0.5 and 0.6. The aim was to take the results into consideration if the intersection point between the estimated

and actual values was greater than these values. First, the results obtained from the 0.5 threshold value are given in Table 2.

Table 2. Results of models (threshold: 0.5)

U-net	**Training Data**		**Test Data**	
Model	**Jaccard Index**	**Dice Coefficient**	**Jaccard Index**	**Dice Coefficient**
resnet34	0.8976	0.9354	0.8563	0.9213
resnet50	0.8716	0.9075	0.8223	0.8872
resnet101	0.8939	0.9361	0.8449	0.9146
effnetb0	0.9028	0.9366	0.8554	0.9212
effnetb1	0.9078	0.9426	0.8579	0.9227

LinkNet	**Training Data**		**Test Data**	
Model	**Jaccard Index**	**Dice Coefficient**	**Jaccard Index**	**Dice Coefficient**
resnet34	0.876	0.9187	0.8498	0.9169
resnet50	0.8605	0.9028	0.839	0.9105
resnet101	0.8351	0.8866	0.8382	0.9099
effnetb0	0.8996	0.9363	0.8492	0.9176
effnetb1	0.903	0.9431	0.8611	0.9244

FPN	**Training Data**		**Test Data**	
Model	**Jaccard Index**	**Dice Coefficient**	**Jaccard Index**	**Dice Coefficient**
resnet34	0.9079	0.9429	0.8546	0.9202
resnet50	0.8994	0.9361	0.841	0.9116
resnet101	0.8511	0.9015	0.8403	0.911
effnetb0	0.8887	0.9278	0.8448	0.9145
effnetb1	0.914	0.9495	0.8589	0.9233

When we evaluate the table obtained for threshold value 0.5, it is possible to see the highest Jaccard index and dice coefficient values with the EfficientNet B1 backbone in all segmentation algorithms. If they are evaluated among themselves, FPN reached the highest Dice coefficient value with a value of 0.9495 for the training data. The Jaccard index here is 0.9140. When the values obtained for the test data are examined, the LinkNet algorithm obtains a 0.9244 Dice coefficient value and a 0.8611 Jaccard index value. In Table 3, the results obtained from threshold 0.6 are given.

In the table for threshold 0.6, a 0.9451 Dice coefficient value for training data and a 0.9096 Jaccard index were obtained for the ResNet34 backbone in the FPN model. This value is the highest value for training data. The highest values for the test data were also obtained with the FPN algorithm, but from the EfficientNet B1 backbone. These values are 0.9241 Dice coefficient and 0.8605 Jaccard index values.

Table 3. Results of models (threshold: 0.6)

U-net	**Training Data**		**Test Data**	
Model	**Jaccard Index**	**Dice Coefficient**	**Jaccard Index**	**Dice Coefficient**
resnet34	0.8663	0.9098	0.8364	0.9076
resnet50	0.8976	0.9328	0.8355	0.9081
resnet101	0.8682	0.9161	0.8282	0.9025
effnetb0	0.8995	0.939	0.8521	0.9191
effnetb1	0.8904	0.9295	0.8538	0.92
LinkNet	**Training Data**		**Test Data**	
Model	**Jaccard Index**	**Dice Coefficient**	**Jaccard Index**	**Dice Coefficient**
resnet34	0.8732	0.9127	0.8516	0.9187
resnet50	0.8592	0.9049	0.8288	0.9034
resnet101	0.877	0.9229	0.8511	0.9187
effnetb0	0.8807	0.921	0.8506	0.9178
effnetb1	0.8954	0.9359	0.8563	0.9218
FPN	**Training Data**		**Test Data**	
Model	**Jaccard Index**	**Dice Coefficient**	**Jaccard Index**	**Dice Coefficient**
resnet34	0.9096	0.9451	0.8538	0.9199
resnet50	0.8993	0.9311	0.8476	0.9164
resnet101	0.8695	0.9107	0.8371	0.9086
effnetb0	0.9011	0.9336	0.8535	0.9196
effnetb1	0.8983	0.9339	0.8605	0.9241

The highest results obtained from the training and test data for both threshold values are given in Table 4 and Table 5, respectively.

Table 4. Threshold results for training data

Threshold	**Algorithm**		**Train Data**	
		Model	**Jaccard Index**	**Dice Coefficient**
0.5	FPN	EfficientNetB1	0.914	0.9495
0.6	FPN	Resnet34	0.9096	0.9451

Table 5. Threshold results for test data

			Test Data	
Threshold	**Algorithm**	**Model**	**Jaccard Index**	**Dice Coefficient**
0.5	LinkNet	EfficientNetB1	0.8611	0.9244
0.6	FPN	EfficientNetB1	0.8605	0.9241

When we examine the table comparing the threshold values, the FPN algorithm with a 0.5 threshold and the EfficientNet B1 backbone training data obtained the highest values with a 0.9495 Dice coefficient and a 0.9140 Jaccard index. In the test data, the highest values were obtained at the 0.5 threshold. These values were obtained from the LinkNet algorithm and the EfficientNet B1 model. The resulting Jaccard index was 0.8611, and the Dice coefficient value was 0.9244. In Figure 9, the loss charts for the models that provided the best values in the test data are given.

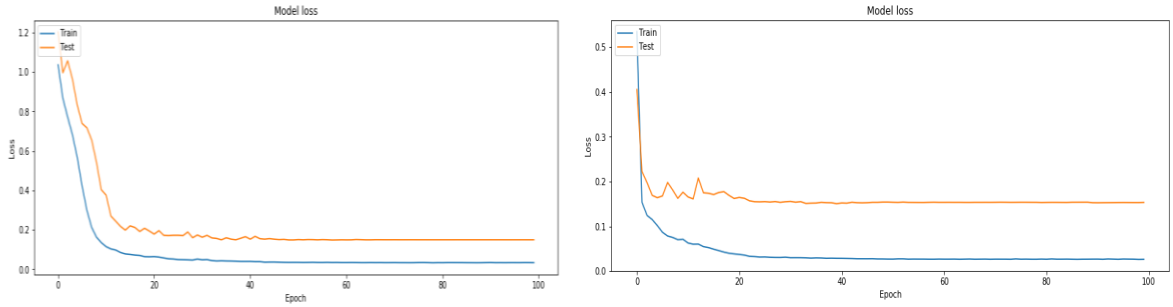

a) LinkNet EfficientNet B1 model loss values (threshold 0.5)

b) FPN EfficientNet B1 model loss values (threshold 0.6)

Figure 9. Loss function values of best models

In Figure 10, some examples of the segmentation results from the algorithms where these values were obtained are shown. The aim was to show the segmentation performance by obtaining segmentation results for the same samples in both models. The first line shows the hospital data, and the second line shows sample data from the RNSA dataset. As can be seen, the images obtained are clearer based on the device quality. Although the picture quality is low in the models we compared, successful results were obtained. While a 0.80 Jaccard index was obtained for LinkNet in the first line image, a 0.70 Jaccard index was obtained for the same image in FPN. For the picture in the second line, a 0.94 Jaccard index was obtained in LinkNet, while a 0.93 Jaccard index was obtained in FPN.

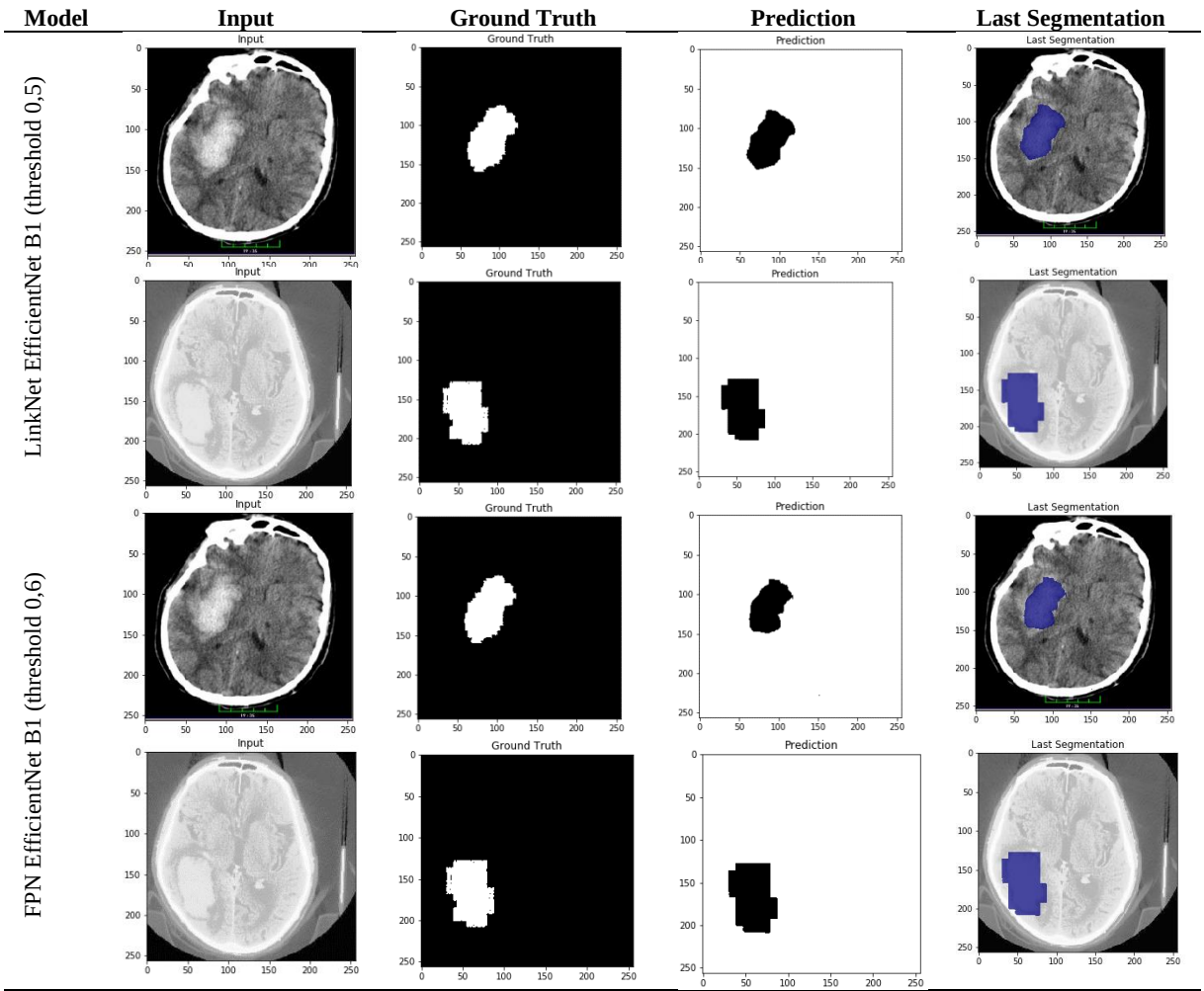

Figure 10. Results of the best models

6. Discussion

Our study started with marking images obtained from the hospital by experts and obtaining the masks with image preprocessing techniques. Cases where the obtained images may be insufficient for the performance of the segmentation algorithms are taken into account. For this reason, new images of intracerebral hemorrhages were taken from the Kaggle database and marked by our experts. The selection of this disease in our study is also important. As reported by the experts where we live, intracerebral hemorrhage is detected more frequently among intracranial hemorrhages. Carrying out the study with three segmentation algorithms is a preliminary process for the web-based software we plan to develop to detect this disease. With the use of our web-based software in hospitals, it will be a decision-support mechanism that will help experts make decisions more quickly.

For these purposes, a detailed examination of segmentation algorithms was made in our study. By adding backbones to the standard structure of these algorithms, it was seen that the features were better extracted, and thus they performed better. EfficientNet, which is used as a backbone in the study, is one of the state-of-the-art deep learning models. Although ResNet is not as new as EfficientNet, it is still a powerful model that is frequently used in studies. This algorithm takes its power from the residual layers of the layers, which provide information from the previous layer. With these layers, information transmission is provided between the layers. It is undesirable to have information lost in feature extraction in medical images. Again, EfficientNet is one of the current models that has found a solution to this problem. Therefore, in this study, we wanted to compare the strong results of the models over time by taking an old and a new model.

In Section 2, studies for ICH classification and segmentation are discussed separately. While examining the studies, explanations were given about their limitations and how our study dealt with these limitations. For example, in [24], it was reported that small hemorrhages could not be detected and an incorrect segmentation process occurred due to density similarity. In our study, it was reported that even small hemorrhages could be easily detected, according to the determination of our experts. Arab et al. reported that erroneous results may be obtained as a result of human-induced markings in the dataset [19]. We tried to minimize the error rate by labeling the datasets of the three experts in our study and validating them separately. In addition, in the studies we examined, after using image processing techniques on images, segmentation or classification was made. With the backbones we used and the extraction of features, there was no need for any image processing before the training.

When the results of our study are examined, looking at the values obtained from the three segmentation algorithms, it is possible to say that the FPN algorithm achieves better results than the other algorithms, considering the metrics accepted for intracerebral hemorrhage segmentation. As we know, many deep learning models are used as backbones in the background of these algorithms. In this study, we chose different versions of the ResNet and EfficientNet models as backbones. In summary, our study covers three segmentation algorithms and five backbones. Among these backbones, EfficientNet models achieved better results. Additionally, with the models developed, our approach will have the advantage of further speeding up the pre-processing step that requires an expert so that the patient can be intervened with more quickly.

In Section 2, where segmentation studies in different fields are examined, segmentation performance above 90% was not achieved in most of the studies related to ICH. In our study, there was a success rate of 0.9495. Considering the results obtained and the studies we examined in the literature, it was confirmed by our experts that better results were obtained in the detection of intracerebral hemorrhage with the models we developed. In addition, the segmentation architectures used in our study and studies using multiple backbones were not encountered in the literature at the time of this study. It motivated us to include different architectures in our study and to add the performance results of different backbones used with these architectures to the literature. Another result encountered while examining previous studies was that the studies were not used as software; in other words, they were not practically included in clinical studies. For this purpose, the necessary models were created for our web-based ICH detection software, which we will present in our future studies.

In addition, as mentioned in the dataset introduction, our work achieved successful results even with the RNSA dataset, which consists of low-quality images. This is noteworthy in terms of demonstrating the power of segmentation algorithms and their backbones. The dataset we labeled in the study will be shared publicly, and other researchers will benefit from it. We think that this will be another contribution of our study to the field.

As is known, deep learning applications have high computational costs. When GPU graphics cards are used, operations are performed in a very short time. If the calculation times in the study are investigated, each epoch lasted between 10 and 30 seconds in our study. The shorter this period, the earlier the disease can be detected, and thus the patient can be intervened in in a short time.

7. Conclusions

In this study, we attempted to demonstrate the performance of three different segmentation algorithms for the segmentation of intracerebral hemorrhage detection. An original dataset obtained from the hospital and marked by experts was prepared for the study. In addition, this dataset was enriched with images of this disease obtained from the Kaggle platform. For the backbone selection of the models, the ResNet and EfficientNet deep learning models were chosen. A total of five backbones were used. When the results were examined, the FPN model provided better results for the training data, and the LinkNet model provided better results for the test data. When a comparison is made between backbones, EfficientNet models give better results than ResNet models. The results were evaluated by experts, and it is predicted that it will be a decision-support mechanism that helps expert opinion in hospitals. It has led us to predict that our study can be used objectively in clinical applications after the results were verified separately by three experts. In addition to this foresight, we are aware that better models can emerge by making performance evaluations and receiving feedback with each new piece of data received. For this purpose, the aim is to transfer this study to a web platform for future studies and to continue testing in the hospital environment. We consider this original study a suitable option when rapid diagnosis or a second opinion is required for the detection of intracranial hemorrhage. With the publication of the dataset prepared for the application, a unique dataset will be included in the literature. In addition, we continue to work on other intracranial hemorrhage detection models.

8. Author Contribution Statement

Murat CANAYAZ: Methodology, Software, Validation, Investigation, Data curation, Writing - original draft, Visualization, Project administration, Conceptualization, Validation, Formal analysis, Resources, Writing - review & editing, Supervision, Visualization. Aysel Milanlıoğlu: Writing - original draft, Visualization, Writing - review & editing, Validation, Resources, Formal analysis, Investigation. Sanem Şehribanoğlu: Visualization, Project administration, Conceptualization, Validation, Formalanalysis, Resources, Writing - review & editing, Supervision, Visualization. Abdulsabır Yalın: Writing - original draft, Visualization, Writing - review & editing, Validation, Resources, Formal analysis, Investigation. Adem Yokuş: Writing - original draft, Visualization, Writing - review & editing, Validation, Resources, Formal analysis, Investigation.

9. Ethics Committee Approval and Conflict of Interest

In our study, the data of 100 patients (44 males, 56 females) diagnosed with SIH, who were hospitalized in the Neurology Department of Van Yuzuncu Yıl University, were analyzed retrospectively. All permissions for the study were obtained from the hospital ethics committee. There is no conflict of interest with any person/institution in the prepared article.

10. References

[1] M.U. Rehman, S. Cho, J.H. Kim and K.T. Chong, "Bu-net: Brain tumor segmentation using modified u-net architecture", Elect., 9, 1-12, 2020.
[2] T. Lan, Y. Li, J.K. Murugi, Y. Ding and Z. Qin, "RUN:Residual U-Net for Computer-Aided Detection of Pulmonary Nodules without Candidate Selection", http://arxiv.org/abs/1805.11856, 2018.
[3] R.L. Araújo, F.H.D. de Araújo and R.R.V. Silva, Automatic segmentation of melanoma skin cancer using transfer learning and fine-tuning, Multimed. Syst., 2021.
[4] Q. Chen, P. Liu, J. Ni, Y. Cao, B. Liu and H. Zhang, "Pseudo-Labeling for Small Lesion Detection on Diabetic Retinopathy Images", Int. Jt. Conf. Neural Networks, IEEE, pp. 1–8, 2020.
[5] C.J. J van Asch, M.J. A Luitse, G.J. E Rinkel, I. van der Tweel, A. Algra and C.J. M Klijn, "Incidence, case fatality, and functional outcome of intracerebral haemorrhage over time, according to age, sex, and ethnic origin: a systematic review and meta-analysis", Lancet Neurol., 9, 167–176, 2010.
[6] M.T.C. Poon, A.F. Fonville and R. Al-Shahi Salman, "Long-term prognosis after intracerebral haemorrhage: systematic review and meta-analysis", J. Neurol. Neur., Psych., 85, 660– 667, 2014.
[7] M. Yamada, "Cerebral amyloid angiopathy: emerging concepts", J. Stroke. 17, 17–30, 2015.
[8] W.C. Ziai and J.R. Carhuapoma, "Intracerebral Hemorrhage., Continuum (Minneap. Minn)", 24, 1603–1622, 2018.
[9] V. Aiyagari, "The clinical management of acute intracerebral hemorrhage", Expert Rev. Neurother. 15, 1421–1432, 2015.
[10] A.I. Qureshi, S. Tuhrim, J.P. Broderick, H.H. Batjer, H. Hondo and D.F. Hanley, "Spontaneous intracerebral hemorrhage", N. Engl. J. Med. 344, 1450–1460, 2001.
[11] O. Flower and M. Smith, "The acute management of intracerebral hemorrhage", Curr. Opin. Crit. Care. 17, 106–114, 2011.
[12] J.C. 3rd Hemphill, S.M. Greenberg, C.S. Anderson, K. Becker, B.R. Bendok, M. Cushman, G.L. Fung, J.N. Goldstein, R.L. Macdonald, P.H. Mitchell, P.A. Scott, M.H. Selim and D. Woo, "Guidelines for the Management of Spontaneous Intracerebral Hemorrhage: A Guideline for Healthcare Professionals From the American Heart Association/American Stroke Association",. 46 2032–2060, 2015.
[13] Kaggle, RSNA Intracranial Hemorrhage Detection, https://www.kaggle.com/c/rsna-intracranial-hemorrhage-detection/data, 2021.
[14] M.I. Aguilar and T.G. Brott, "Update in intracerebral hemorrhage", The Neurohosp., 1, 148–159, 2011.
[15] A. Patel, F.H.B.M. Schreuder, C.J.M. Klijn, M. Prokop, B. van Ginneken, H.A. Marquering, Y.B.W.E.M. Roos, M.I. Baharoglu, F.J.A. Meijer and R. Manniesing, "Intracerebral haemorrhage segmentation in non-contrast CT. ", Sci. Rep. 9, 17858, 2019.
[16] J. Xu, R. Zhang, Z. Zhou, C. Wu, Q. Gong, H. Zhang, S. Wu, G. Wu, Y. Deng, C. Xia and J. Ma, "Deep network for the automatic segmentation and quantification of ıntracranial hemorrhage on CT", Front. Neurosci. 14, 1084, 2021.
[17] K. Hu, K. Chen, X. He, Y. Zhang, Z. Chen, X. Li and X. Gao, "Automatic segmentation of intracerebral hemorrhage in CT images using encoder–decoder convolutional neural network", Infor. Process. & Manag., 57, 102352, 2020.
[18] T. Falk, D. Mai, R. Bensch, Ö. Çiçek, A. Abdulkadir, Y. Marrakchi, A. Böhm, J. Deubner, Z. Jäckel, K. Seiwald, A. Dovzhenko, O. Tietz, C. Dal Bosco, S. Walsh, D. Saltukoglu, T.L. Tay, M. Prinz, K. Palme, M. Simons, I. Diester, T. Brox and O. Ronneberger, "U-Net: deep learning for cell counting, detection, and morphometry", Nat. Methods. 16, 67–70, 2019.
[19] A. Arab, B. Chinda, G. Medvedev, W. Siu, H. Guo, T. Gu, S. Moreno, G. Hamarneh, M. Ester and X. Song, "A fast and fully-automated deep-learning approach for accurate hemorrhage segmentation and volume quantification in non-contrast whole-head CT", Sci. Rep. 10, 19389, 2020.
[20] S. Jadon, O.P. Leary, I. Pan, T.J. Harder, D.W. Wright, L.H. Merck and D. Merck, "A comparative study of 2D image segmentation algorithms for traumatic brain lesions using CT data from the ProTECTIII multicenter clinical trial", in: T.M. Deserno, P.-H. Chen (Eds.), Imaging Informatics

Heal. Res. Appl., SPIE, p. 48, 2020.
[21] G. Cao, Y. Wang, X. Zhu, M. Li, X. Wang and Y. Chen, "Segmentation of İntracerebral Hemorrhage Based on İmproved U-Net", in: 2020 IEEE Conf. Telecommun. Opt. Comput. Sci., IEEE, pp. 183–185, 2020.
[22] J.L. Wang, H. Farooq, H. Zhuang and A.K. Ibrahim, "Segmentation of Intracranial Hemorrhage Using Semi-Supervised Multi-Task Attention-Based U-Net", Appl. Sci. 10, 2020.
[23] B.S. Maya and T. Asha, "Segmentation and classification of brain hemorrhage using U-net and CapsNet", J. Seybold Rep. 1, 18–25, 2020.
[24] M.D. Hssayeni, M.S. Croock, A. Al-Ani, H.F. Al-Khafaji, Z.A. Yahya and B. Ghoraani, "Intracranial Hemorrhage Segmentation Using Deep Convolutional Model, (n.d.).
[25] V. Abramova, A. Clèrigues, A. Quiles, D.G. Figueredo, Y. Silva, S. Pedraza, A. Oliver and X. Lladó, "Hemorrhagic stroke lesion segmentation using a 3D U-Net with squeeze-and-excitation blocks", Comput. Med. Imaging Graph. 90, 101908, 2021.
[26] Y. Liu, Q. Fang, A. Jiang, Q. Meng, G. Pang and X. Deng, "Texture analysis based on U-Net neural network for intracranial hemorrhage identification predicts early enlargement", Comput. Methods Programs Biomed. 206, 106140, 2021.
[27] C. Sai Manasa and V. Bhavana, "Deep Learning Algorithms to Detect and Localize Acute Intracranial Hemorrhages", in: Sabu M. Thampi, Sri Krishnan, Rajesh M. Hegde, Domenico Ciuonzo, Thomas Hanne, Jagadeesh Kannan R. (Eds.), Adv. Signal Process. Intell. Recognit. Syst., Springer, Singapore, 367–374, 2021.
[28] J. He, "Automated Detection of Intracranial Hemorrhage on Head Computed Tomography with Deep Learning", in: Proc. 2020 10th Int. Conf. Biomed. Eng. Technol., ACM, New York, NY, USA, 117–121, 2020.
[29] S. Castro, Juan Sebastian Chabert, C. Saavedra and R. Salas, "Convolutional neural networks for detection intracranial hemorrhage in CT images", in: CEUR Workshop Proc., 37–43, 2020.
[30] M. Burduja, R.T. Ionescu and N. Verga, "Accurate and efficient ıntracranial hemorrhage detection and subtype classification in 3d ct scans with convolutional and long short-term memory neural networks", Sensors. 20, 5611, 2020.
[31] S. Ghosh and K.C. Santosh, "Tumor Segmentation in Brain MRI: U-Nets versus Feature Pyramid Network", IEEE 34th Int. Symp. Comput. Med. Syst., IEEE, 2021.
[32] Z. Sobhaninia, A. Emami, N. Karimi and S. Samavi, "Localization of Fetal Head in Ultrasound Images by Multiscale View and Deep Neural Networks", 25th Int. Comput. Conf. Comput. Soc. Iran, IEEE, 2020.
[33] D. Fan, C. Zhang, B. Lv, L. Wang, G. Wang, M. Wang, C. Lv and G. Xie, "Positive-Aware Lesion Detection Network with Cross-scale Feature Pyramid for OCT Images", 2020.
[34] X. Dai, Y. Lei, T. Wang, A.H. Dhabaan, M. McDonald, J.J. Beitler, W.J. Curran, J. Zhou, T. Liu and X. Yang, "Head-and-neck organs-at-risk auto-delineation using dual pyramid networks for CBCT-guided adaptive radiotherapy", Phys. Med. Biol. 66, 2021.
[35] J. Lo, S. Nithiyanantham, J. Cardinell, D. Young, S. Cho, A. Kirubarajan, M.W. Wagner, R. Azma, S. Miller, M. Seed, B. Ertl-Wagner and D. Sussman, "Cross Attention Squeeze Excitation Network (CASE-Net) for Whole Body Fetal MRI Segmentation", Sensors. 21, 4490, 2021.
[36] J. Singh, A. Tripathy, P. Garg and A. Kumar, "Lung tuberculosis detection using anti-aliased convolutional networks", Procedia Comput. Sci. 173, 281–290, 2020.
[37] J. Long, E. Shelhamer and T. Darrell, "Fully convolutional networks for semantic segmentation, IEEE Conf. Comput. Vis. Pattern Recognit., IEEE, 2015.
[38] O. Ronneberger, P. Fischer and T. Brox, "U-Net: Convolutional Networks for Biomedical Image Segmentation", N. Navab, J. Hornegger, W.M. Wells, A.F. Frangi (Eds.), Med. Image Comput. Comput. Interv. – MICCAI 2015, Lecture Notes in Computer Science, vol 9351.Springer, Munich, Germany, 234–241, 2015.
[39] L. Jiao and J. Zhao, "A survey on the new generation of deep learning in ımage processing", IEEE Access. 7, 2019.
[40] L. Li, M. Wei, B. Liu, K. Atchaneeyasakul, F. Zhou, Z. Pan, S.A. Kumar, J.Y. Zhang, Y. Pu, D.S. Liebeskind and F. Scalzo, "Deep learning for hemorrhagic lesion detection and segmentation on brain CT Images", IEEE J. Biomed. Heal. Informatics. 25, 2021.
[41] G. Cao, Y. Wang, X. Zhu, M. Li, X. Wang and Y. Chen, "Segmentation of intracerebral hemorrhage

based on improved U-Net, IEEE Conf. Telecommun. Opt. Comput. Sci., IEEE, pp. 183–185, 2020.
[42] M.G. Oghli, A. Shabanzadeh, S. Moradi, N. Sirjani, R. Gerami, P. Ghaderi, M. Sanei Taheri, I. Shiri, H. Arabi and H. Zaidi, "Automatic fetal biometry prediction using a novel deep convolutional network architecture", Phys. Medica. 88, 127–137, 2021.
[43] A. Chaurasia and E. Culurciello, "LinkNet: Exploiting Encoder Representations for Efficient Semantic Segmentation", 2017.
[44] Z. Sobhaninia, S. Rezaei, N. Karimi, A. Emami and S. Samavi, "Brain Tumor Segmentation by Cascaded Deep Neural Networks Using Multiple Image Scales", 28th Iran. Conf. Electr. Eng., IEEE, 2020.
[45] S.S. Seferbekov, V.I. Iglovikov, A. V. Buslaev and A.A. Shvets, "Feature Pyramid Network for Multi-Class Land Segmentation", http://arxiv.org/abs/1806.03510, 2018.
[46] E.H. Adelson, C.H. Anderson, J.R. Bergen, P.J. Burt and J.M. Ogden, "Pyramid methods in image processing", RCA Eng. 29, 33–41. http://persci.mit.edu/pub_pdfs/RCA84.pdf, 1984.
[47] T.-Y. Lin, P. Dollar, R. Girshick, K. He, B. Hariharan and S. Belongie, "Feature Pyramid Networks for Object Detection", IEEE Conf. Comput. Vis. Pattern Recognit., IEEE, pp. 936–944, 2017.
[48] M. Hu, Y. Li, L. Fang and S. Wang, "A2-FPN: Attention Aggregation Based Feature Pyramid Network for Instance Segmentation", in: Proc. IEEE/CVF Conf. Comput. Vis. Pattern Recognit., pp. 15343–15352, 2021.
[49] K. He, X. Zhang, S. Ren and J. Sun, "Deep Residual Learning for Image Recognition", arXiv:1512.03385v1 (n.d.) 1–12. http://image-net.org/challenges/LSVRC/2015/, 2021.
[50] M. Gao, J. Chen, H. Mu, D. Qi, "A transfer residual neural network based on resnet-34 for detection of wood knot defects", Fores., 12, 1–16, 2021.
[51] M. Tan and Q. V. Le, "EfficientNet: Rethinking Model Scaling for Convolutional Neural Networks", arXiv:1905.11946v5, http://arxiv.org/abs/1905.11946, 2019.
[52] T.Y. Lin, P. Goyal, R. Girshick, K. He and P. Dollar, "Focal loss for dense object detection", IEEE Trans. Pattern Anal. Mach. Intell. 42, 318–327, 2020.